PHYSICAL REVIEW B **85**, 220102(R) (2012)

Direct extraction of quantitative structural information from x-ray fluorescence holograms using spherical-harmonic analysis

Yuhao Wang,[1] Jianming Bai,[2] and Trevor A. Tyson[1]
[1]*Department of Physics, New Jersey Institute of Technology, Newark, New Jersey 07102, USA*
[2]*National Synchrotron Light Source, Brookhaven National Laboratory, Upton, New York 11073, USA*
(Received 16 November 2011; revised manuscript received 14 March 2012; published 12 June 2012)

An x-ray fluorescence holograph contains information on both the amplitude and the phase of the x-ray scattering signal from a crystal structure. X-ray fluorescence holography is potentially a technique to directly extract atomic level structure information from crystal samples. We present here a reconstruction algorithm using a spherical-harmonic analysis that significantly improves the structure-resolving power of x-ray fluorescence holography over the widely used multiple energy Barton transform approach. Compared to the direct method for x-ray diffraction, this direct method has the advantages of full model independence and applicability to crystal systems with a large contrast in atomic numbers.

DOI: 10.1103/PhysRevB.85.220102 PACS number(s): 61.05.cc, 02.30.Zz, 07.05.Kf, 42.40.Kw

X-ray fluorescence holography (XFH) is a promising technique for model-independent structure determination from single crystals. Unlike standard x-ray diffraction (XRD) methods that measure only the magnitude of the structure factors and require significant *a priori* knowledge of the crystal structure for generating a solution, XFH is sensitive to both the amplitude and phase of the structure factor. However, even though the experimental XFH measurement was realized 15 years ago,[1,2] and data collection procedures have greatly improved with the advent of high flux third generation synchrotron sources, effective methods for retrieving quantitative structural information from x-ray holograms are still needed.

The complete structural information of a crystal can be represented by a three-dimensional (3D) density distribution of electron charge, or its Fourier transformation in the reciprocal space, viz., structure factors. The electron density is a fundamental physical property of an electronic system. As stated in the Hohenberg-Kohn theorem,[3] the ground state energy and all other observables of the system are uniquely determined by the density. Hence, establishment of an experimental method that directly measures the electron density distribution of a crystal structure will be an important progress in solid state physics. The current direct methods of x-ray crystallography assume that the crystals consist of discrete atoms,[4] and thus provide electron densities limited by the isolated-atom approximation. The derivation of a more realistic electron density that reflects the charge localization arising from chemical bonding still relies on model building and refinements.[5] We will introduce a reconstruction algorithm for XFH data that can retrieve the electron density directly without a discrete atom assumption.

Previous work widely used the Barton transform method,[6] an atomic image reconstruction algorithm based on the Helmholtz-Kirchhoff integral theorem, for analyzing XFH data. The 3D image calculated with the Barton transform method is the wave field amplitude around the fluorescence emitting atoms formed by a fictitious converging spherical wave through the recorded hologram. This image assumes maxima at atomic positions, but is distorted because of interference between the scattered waves. The interference artifacts can be suppressed by summing multiple energy XFH data.[2] However, the resulting image differs significantly from the true charge density of a material. Typically, it is extremely difficult, if not impossible, to solve unknown structures or to do any quantitative structural analysis with XFH data using the Barton transform technique.

Much effort has been invested in developing methods to extract the electron density directly from an XFH measurement. Chukhovskii *et al.*[7] proposed a Fourier transform type algorithm to derive the distribution of electron charge density from XFH data. Their results using a single wavelength hologram are similar to, but have better spatial resolution than, those obtained with the Barton transform method. Seemingly, the algorithm can restore the true electron charge density from data taken with a suitably large energy range, however, this is impractical with current experimental approaches. Marchesini *et al.*[8] proposed an iterative image deconvolution method to construct the electron charge density from XFH data. They demonstrated the method by approximating the atoms in the crystal as point charges. However, it is questionable that their iterative procedure will converge to the true electron charge density. Matsushita *et al.*[9,10] developed the scattering pattern matrix (SPM) method to derive a 3D atomic distribution function defined in real space from the two-dimensional (2D) hologram taken in **k** space with the iterative-scaling algorithm of maximum entropy. By using the non-negative constraint, and imposing translational symmetry of the atomic distribution function, they successfully reconstructed atomic images from measured XFH holograms without significant artifacts. Most recently, the SPM method has been successfully used to reconstruct 3D atomic images of a $SrTiO_3$ crystal from multiple energy internal-detector electron holography data.[11] This fitting-based reconstruction algorithm requires atomic information of a unit cell before solving the structure. Chukhovskii *et al.*[12,13] defined a scattering function connecting the XFH hologram function to the structure factors. Using standard least square methods, they retrieved a set of structure factors from an XFH hologram simulated with the same set of structure factors. This formalism needs to be tested with more realistic model holograms based on real space atomic configurations. As we indicate later, each XFH hologram can be expressed by a complete set of structure factors with a finite number limited by the energy of the scattered waves.

A complete set of structure factors is needed to avoid truncation errors in the XFH structure analysis.

In order to solve an unknown structure using XFH data, we developed a formalism connecting the structure factors to the spherical-harmonic components of XFH holograms via a set of linear equations. The electron density then is obtained by Fourier expansion, using the structure factors resolved by directly solving the linear equations. The major differences between our algorithm and previous methods are as follows: First, ours provides a better way to sample the XFH data in **k** space. A spherical harmonic is essentially a Fourier transformation on a spherical surface; a finite number of spherical-harmonic coefficients contain all structural information in a set of XFH data. The advantage of using a spherical-harmonic expansion lies in the fact that each spherical-harmonic component represents a weighted integration of the hologram on the surface of a sphere in **k** space, analogous to the integrated intensity of the Bragg peaks in x-ray diffraction. As Warren[14] noted, intensity as function of the diffraction angle usually is not an observable quantity; rather the integrated intensity is more useful since it can be both calculated and measured. In XFH, each spherical-harmonic component of the hologram is a well defined quantity, expressible as a linear expansion of structure factors with a well behaved scattering matrix. Therefore, the second advantage of our algorithm over previous methods is that it solves the structure model independently without any fitting or iteration procedures. We demonstrate below that using the spherical-harmonic method allows us to retrieve the structure factors from holograms simulated with real space atomic configurations, and with these structure factors, the electron charge density can be reconstructed with high fidelity.

The x-ray fluorescence hologram for a polarized probing wave can be expressed[15,16] as

$$\chi(\vec{k}) = -\iiint \rho(\vec{r})\frac{r_e \exp(ikr - i\vec{k}\cdot\vec{r})}{\mathrm{r}} \times [A(kr) + B(kr)(\varepsilon\cdot\hat{r})^2]d\vec{r} + \text{c.c.}, \quad (1)$$

where $\chi(\vec{k})$ represents holograph χ in **k** space, $\rho(\vec{r})$ is the electron density distribution in real space, r_e is the classical electron radius (e^2/mc^2), $[A(kr) + B(kr)(\varepsilon\cdot\hat{r})^2]$ is a generalized expression for the scattering factor between the polarized photon and electron, ε is the direction of the electric field, and $\hat{r}$ is the direction of $\vec{r}$. Considering a near field effect (the deviations from plane wave behavior of the probing waves), $A(kr) = \frac{i}{kr} - \frac{1}{(kr)^2} + 1$ and $B(kr) = -\frac{3i}{kr} + \frac{3}{(kr)^2} - 1$. $\vec{r}$ represents the position of the scattering electron relative to the fluorescent center at $\vec{r} = 0$. Most complex crystal structures encompass multiple fluorescent atomic sites with a unique atomic distribution in a unit cell. The experimentally measured hologram $\chi(\vec{k})$ from these structures is a superposition of fluorescence patterns from different fluorescent atomic sites, and the $\rho(\vec{r})$ in Eq. (1) should be the averaged electron charge distribution with respect to all unique fluorescent atomic sites of the same chemical species. In this Rapid Communication, the term "electron density" refers to its averaged value when multiple fluorescent atomic sites are involved.

The hologram $\chi(\vec{k})$ is usually represented as $\chi(\theta,\varphi)$ for a fixed wave number **k**, where (θ,φ) is the direction of $\vec{k}$, as represented in a spherical coordinate system of measurement.

In transverse waves such as x rays, the polarization vector ε is always in a plane perpendicular to the wave vector **k**. In the direct scheme XFH the unpolarized fluorescence wave is the probing wave and the ε in Eq. (1) is averaged in the plane. Equation (1) can be simplified as

$$\chi(\vec{k}) = \iiint \rho(\vec{r})\frac{r_e \exp(ikr - i\vec{k}\cdot\vec{r})}{r} \times \left\{A(r) + \frac{B(r)}{2}[1 - (\hat{k}\cdot\hat{r})^2]\right\}d\vec{r} + \text{c.c.} \quad (2)$$

For the indirect scheme XFH, the probing wave is the polarized, elastically scattered x-ray wave. The indirect XFH can be depolarized by summing the holograms measured with two perpendicular polarization directions, $\varepsilon_\perp$ and $\varepsilon_\parallel$. With $(\varepsilon_\perp\cdot\hat{r})^2 + (\varepsilon_\parallel\cdot\hat{r})^2 + (\hat{k}\cdot\hat{r})^2 = 1$, the depolarized indirect XFH also can be represented by Eq. (2). The following discussions apply to both direct XFH and depolarized indirect XFH, as described by Eq. (2).

Equation (2) resembles the Fredholm integral equation of first kind commonly encountered in typical inverse problems. However, here the observed hologram $\chi(\vec{k})$ is only the real part of the integral function and is defined on a sphere surface in **k** space. In previous works, such as in Ref. 8, the discrete points of the hologram were used to solve the integral equation. The resulting system of linear equations was usually ill conditioned and must be solved using least square methods.

To extract the electron density from XFH, we expand the hologram with respect to spherical harmonics, and derive a relation between the spherical harmonic coefficients and the electron density function.

By replacing the expression for the plane wave with a spherical wave expansion in Eq. (2),

$$\exp(-i\vec{k}\cdot\vec{r}) = \sum_{l=0}^{\infty}(-i)^l(2l+1)j_l(kr)P_l(\hat{k}\cdot\hat{r}), \quad (3)$$

where j_l is the spherical Bessel function and P_l the Legendre function, the hologram χ can then be expanded to

$$\chi = r_e\sum_{l=0}^{\infty}\iiint \rho(\vec{r})\frac{e^{ikr}}{r}S_l(kr)P_l(\hat{k}\cdot\hat{r})d\vec{r} + \text{c.c.} \quad (4)$$

Here, $S_l(kr)$ is a spherical representation of the scattering factor between electrons and photons. Considering a near field effect, $S_l(kr)$ is written as

$$\begin{aligned} S_l(kr) = {} & (-i)^l(2l+1)j_l(kr)\left[\frac{-i}{kr} + \frac{1}{(kr)^2} + 1\right] \\ & + (-i)^l\frac{l(l-1)}{2l-1}j_{l-2}(kr)\left[\frac{-3i}{kr} + \frac{3}{(kr)^2} - 1\right] \\ & - (-i)^l\left[\frac{(l+1)^2}{2l+3} + \frac{l^2}{2l-1}\right]j_l(kr)\left[\frac{-3i}{kr} + \frac{3}{(kr)^2} - 1\right] \\ & + (-i)^l\frac{(l+1)(l+2)}{2l+3}j_{l+2}(kr)\left[\frac{-3i}{kr} + \frac{3}{(kr)^2} - 1\right]. \end{aligned} \quad (5)$$

Also considering $P_l(\hat{k}\cdot\hat{r}) = \frac{4\pi}{2l+1}\sum_{m=-l}^{l} Y_{lm}(\theta_k,\varphi_k)Y_{lm}^*(\theta_r,\varphi_r)$, the spherical-harmonic expansion of the hologram is given by

$$\chi = \sum_{l=0}^{\infty}\sum_{m=-l}^{l} Y_{lm}(\theta_k,\varphi_k)a_{lm} + \text{c.c.}, \tag{6}$$

where a_{lm} is calculated as

$$a_{lm} = \frac{4\pi r_e}{2l+1}\iiint \rho(\vec{r})\frac{e^{ikr}}{r}S_l(kr)Y_{lm}^*(\theta_r,\varphi_r)d\vec{r}. \tag{7}$$

The integral in Eq. (7) extends over the entire volume of a single crystal. The finite crystal size can be represented by a periodical $\rho(\vec{r})$ in infinite 3D space multiplied with an envelope size distribution function $\mu(r)$. By using the translation symmetry of the crystal, the electron density can be written as $\rho(\vec{r}) = \sum \rho(\vec{h})\exp(i\vec{h}\cdot\vec{r})\mu(r)$, where $\rho(\vec{h})$ is related to the atomic structure factor $F(\vec{h})$ by $\rho(\vec{h}) = F(\vec{h})/V$ (V = unit cell volume). A simple form of $\mu(r)$ is a unit step function $\mu = \eta(r - r_0)$, where r_0 is the average crystal size.

Then, Eq. (7) can be rewritten as

$$a_{lm} = \frac{(4\pi)^2}{2l+1}(i)^l\sum_h [Y_{lm}^*(\theta_h,\varphi_h) \times \int j_l(hr)e^{ikr}\mu(r)S_l(kr)rdr]\rho(\vec{h}). \tag{8}$$

Now we consider the complex conjugate of Eq. (6), and add it to the expression of hologram as a real function:

$$\chi = \sum_{l=0}^{\infty}\sum_{m=-l}^{l} Y_{lm}(\theta_k,\varphi_k)[a_{lm} + (-1)^m a_{l-m}^*] = \sum_{l=0}^{\infty}\sum_{m=-l}^{l} Y_{lm}(\theta_k,\varphi_k)c_{lm}. \tag{9}$$

The c_{lm}'s are the coefficients of spherical harmonics that can be calculated directly from the experimental hologram data. Since the hologram χ is a real function, there are only $l+1$ independent spherical-harmonic coefficients for each l. The c_{lm} coefficients provide a series of linear equations related to the structure factors:

$$c_{lm} = \sum_h \left[\frac{8\pi^2 i^l}{2l+1}Y_{lm}^*(\theta_h,\varphi_h)\int j_l(hr)e^{ikr}S_l(kr)\mu(r)rdr\right]\rho(\vec{h}) + \sum_h \left[\frac{8\pi^2 i^l}{2l+1}Y_{lm}^*(\theta_h,\varphi_h)\int j_l(hr)e^{-ikr} \times S_l^*(kr)\mu(r)rdr\right]\rho(\overrightarrow{-h})^*. \tag{10}$$

Neglecting the anomalous scattering factors by assuming $\rho(\vec{h}) = \rho(\overrightarrow{-h})^*$ [or equivalently, assuming a real electron density function in Eq. (7)], the spherical-harmonic expansion coefficient of the hologram can be given as

$$c_{lm} = \sum_h \left\{\frac{16\pi^2 i^l}{2l+1}Y_{lm}^*(\theta_h,\varphi_h)\int j_l(hr)\text{Re}[e^{ikr} \times S_l(kr)]\mu(r)rdr\right\}\rho(\vec{h}). \tag{11}$$

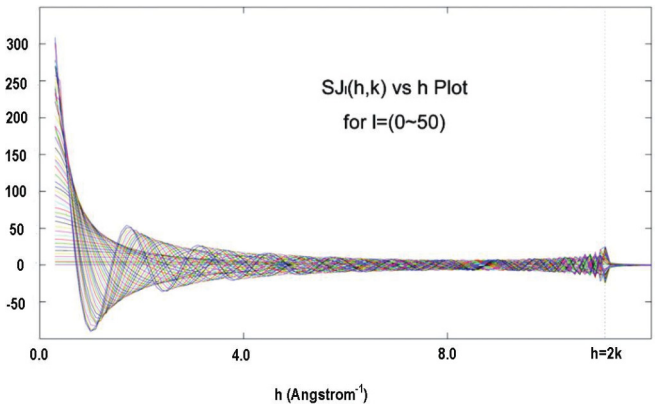

FIG. 1. (Color online) Matrix calculation as a function of h for $k = 5.55$ Å^{-1}.

The structure factors $\rho(\vec{h})$ can be extracted from the coefficients of the spherical harmonics by solving the linear equations (10) or (11). To calculate the matrix elements, we need to know the values of h, θ_h, and φ_h. These are constants related to the lattice parameters, and can be obtained with routine x-ray diffraction measurements or Kossel line measurements on single crystals.[17] We also need to estimate the crystal size from the line broadening of the x-ray diffraction to construct the size distribution function $\mu(r)$.

The integral function in Eq. (11),

$$SJ_l(h,k) = \int j_l(hr)\text{Re}[e^{ikr}S_l(kr)]\mu(r)rdr, \tag{12}$$

is a structure-independent function of h, with a given wave vector k and a size distribution function $\mu(r)$. For odd l's and large even l's, $SJ_l(h,k)$ abruptly approaches zero at $h = 2k$. This is the consequence of the diffraction limit imposed by the equation $\hat{k}\cdot\hat{h} = h/2k$.

Figure 1 shows an example of the numerical calculation of $SJ_l(h,k)$ for $l \in (0,55)$. Integration is performed with $\mu = \eta(r - 200$ Å$)$. For low even l's, the function extends beyond $h = 2k$, but quickly decays to negligible values. We attribute this to the tails of the Kossel lines with h values nearest to $2k$ from above.

Even though the diffraction limit reduces the number of structure factors that can be derived from the XFH data, it helps in defining a finite set of unknowns to be solved in the linear equations (10) and (11). All structure factors with $h < 2k$ must be included to resolve the $\rho(\vec{h})$'s with high accuracy, while it is safe to ignore the structure factors with $h > 2k$ using selected spherical harmonics.

The fine structure of the experimental XFH data depends on crystal size, the angular resolution of the x-ray beam, and other factors that may distort high-frequency signals in the hologram. For a structure to be reliably solved from the hologram, signals more susceptible to experimental conditions must be separated from those strongly determined by the structure factors. The method of spherical-harmonic expansion separates hologram signals according to their angular frequency, thus allowing unreliable high-frequency signals to be discarded. In practice, low- and mid-frequency signals are

weakly influenced by the crystal size and the angular resolution of the x-ray beam.

The number of structure factors to be resolved in this method only depends on the energy of the probing x-ray wave. Therefore, the higher order spherical harmonics generated by sharp Kossel lines due to a large crystal size can be excluded from the structure solving matrix without losing the structural information. This acts effectively as a low-pass filter for suppressing the nonholographic components, namely, the object-object terms[18] and the secondary yield caused by an extinction effect[19] in XFH data.

The samples most suitable to XFH measurement are crystals close to the ideally imperfect condition, as defined by Warren,[14] so that both the object-object term and the extinction effect can be ignored. In practice, usually the crystals under study are imperfect but not ideally imperfect, and have distributions in size and orientation of their mosaic blocks. The large crystal component and the mosaic clusters with a closely coincided orientation are the origins of the nonholographic contaminations. Both of these two kinds of nonholographic terms manifest their effects as abrupt intensity changes in a very narrow angular region in the center of the Kossel lines, and therefore contribute mostly to the higher order harmonics. It has been demonstrated in previous studies[19] that the scattering from large crystals will also contribute to lower order harmonics. The nonholographic terms in these scattering contributions are negligible as they are mostly from the wide angular regions away from Kossel lines. The experimental techniques that have been widely used to minimize the nonholographic terms before data analysis, such as measuring the integrated intensity with a finite angular resolution or averaging afterward by applying a low-pass filter,[18] and taking the holograms with multiple x-ray energies, are compatible and can be used with the spherical-harmonic analysis method.

To demonstrate the structure-resolving power of the spherical harmonic analysis method on XFH data, we applied it to a hexagonal $HoMnO_3$ structure (space group $P63cm$, $a = 6.1413$ Å, $c = 11.4122$ Å).[20] $HoMnO_3$ is an important multiferroic structure.[21] We choose this system as an example because this noncentrosymmetric system has a complex structure factor and has heavy holmium atoms in its unit cell, which makes it difficult to accurately determine the oxygen positions using the regular XRD method. Calculating the spontaneous polarization of the system based on its structure requires accurate determination of the positions of the oxygen in the unit cell. The manganese in the structure is the fluorescence emitter with 8 keV x rays used as the probing wave. A depolarized indirect hologram is simulated with the equation

$$\chi(\vec{k}) = \sum_i f_g(\vec{k},\vec{r}_i)\frac{r_e \exp(ikr_i - i\vec{k}\cdot\vec{r}_i)}{r_i}\mu(r_i) + \text{c.c.}, \quad (13)$$

where $f_g(\vec{k},\vec{r})$ is a generalized atomic scattering factor that includes the near field effect,[22] the anomalous scattering correction, and the polarization factor. We assigned only one of the six Mn atoms in the $HoMnO_3$ unit cell as the fluorescence emitter in our simulation so that we could compare the reconstructed electron density map directly to that of the model structure. With an x-ray energy of 8 keV, there are 3334 structure factors satisfying $h < 2k$. The hologram was simulated with 0.5° resolution in both θ and φ, resulting in 361×720 data points. We employed FORTRAN codes adapted from SPHEREPACK 3.0 (Ref. 23) to calculate the coefficients c_{lm} of spherical-harmonic expansion from these data points. A complementary error function $\mu = \text{erfc}[(r - 150\ \text{Å})/50\ \text{Å}]$ was used to define the crystalline size in the hologram simulation and in the matrix calculation. The c_{lm}'s with $l \in (21,99)$ and $m \in (0,l)$ were used to construct 4740 complex linear equations (11). The matrix is directly invertible with a moderate condition number 434.5. We used the matrix division function of MATLAB to solve this overdetermined linear system.

The 3344 structure factors we extracted had a standard deviation of approximately 1.8% with respect to the model values. We then constructed an electron density map in the (100) plane of $HoMnO_3$ with these structure factors [Fig. 2(a)]. In Fig. 2(b) we depict the real space images obtained using the Barton transform, from five holograms acquired with equally spaced energies from 8.0 to 9.6 keV [Fig. 2(b)], and a single energy hologram at 8 keV [Fig. 2(c)], on the same contrast scale.

Note that the atomic images by the Barton transform look particularly distorted because of the presence of heavy Ho atoms in the $HoMnO_3$ structure and the low symmetry of

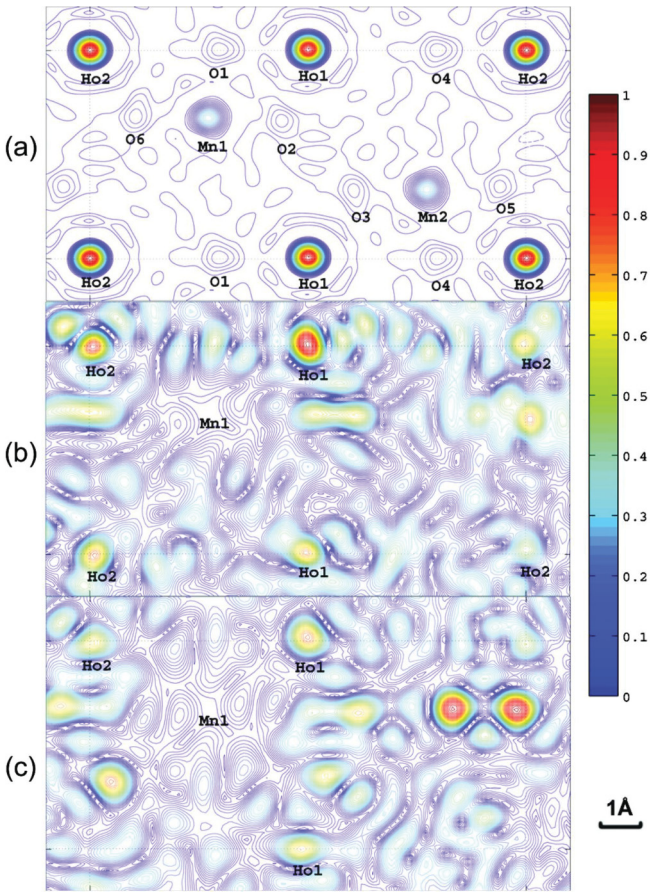

FIG. 2. (Color online) (a) Reconstructed electron density in (100) plane from the solved structural factors of $HoMnO_3$, (b) structure image from Barton's method with five energies, and (c) from Barton's method with one energy.

the $P6_3cm$ space group. The intensity of the interference ripples is proportional to that of the heaviest elements in the structure. The ripples caused by Ho (atomic number 67) are more intense than the image intensity of Mn(25) and O(8) atoms, thus the signal from the Ho dominates the pattern. Because of the low symmetry of the system, the center atom Mn has different distances to the four neighboring Ho atoms in the (100) plane, causing a difference in their image intensities.

Comparing the result of the spherical-harmonic analysis and the Barton transform clearly reveals that our method greatly improved the structure-resolving capability of the XFH method. It also demonstrates that the essential structural information is already contained in a single energy hologram. The electron density map displays precise atomic positions and proper intensity ratios between the Ho, Mn, and O atoms, thus providing adequate information to resolve the structure without *a priori* knowledge of the atomic constituents of the unit cell. Importantly, the position and shape of the oxygen atoms are shown clearly, despite the presence of heavy holmium atoms in the unit cell. Hence, XFH undoubtedly is an effective tool to probe systems with high variations in electron density. Further, the spherical-harmonic analysis on XFH data affords us a method to study the nonspherical distributions of the electron density without resorting to model building or phase refinement. This application of XFH may become a unique tool for x-ray crystallography studies of electron density.

The ambiguity caused by the multiple symmetry distinct fluorescence centers is an intrinsic limit of the XFH method and can be resolved by making use of space group symmetry and bond length constraints. Spherical-harmonic analysis, as well as the Barton transform method, require a hologram data set in a full 4π solid angle. Currently, most XFH measurements are taken from a flat surface of large single crystals, and hence it is difficult to directly measure the hologram in a full 4π solid angle in this geometry. Therefore, the point group symmetry of the crystal is employed to extend the data set to its full range. With the advancements in techniques of synchrotron radiation, XFH can be measured from small crystals in the transmission mode using a highly focused beam. XFH in a transmission mode will make it possible to directly measure the full range hologram, to measure the holograms in two polarization geometries with the same diffractometer setup (to depolarize the direct XFH data), and to extend the application of XFH to other fields of crystallography, such as structural biology.

Our reconstruction algorithm based on spherical-harmonic analysis provides an efficient method that is readily automated to directly extract structural information from single energy x-ray fluorescence holograms. This method makes XFH a quantitative method that is highly applicable to fields of material characterization. Since the method does not rely on the isolated-atom approximation, it can be used to retrieve electron density from high resolution XFH data, and thus provides a benchmark for quantum-chemical calculations based on density functional theory.

This work is supported in part by NSF instrumentation Grant No. DMR MRI-0722730. The authors acknowledge helpful discussions with Yangang Liu on general inverse problems and Weiguo Yin on density functional theory.

[1] M. Tegze and G. Faigel, Nature (London) **380**, 49 (1996).
[2] T. Gog, P. M. Len, G. Materlik, D. Bahr, C. S. Fadley, and C. Sanchez-Hanke, Phys. Rev. Lett. **76**, 3132 (1996).
[3] P. Hohenberg and W. Kohn, Phys. Rev. B **136**, 864 (1964).
[4] H. Hauptman, Science **233**, 178 (1986).
[5] B. Dittrich, T. Koritsanszky, and P. Luger, Angew. Chem. Int. Ed. **43**, 2718 (2004).
[6] J. J. Barton, Phys. Rev. Lett. **61**, 1356 (1988).
[7] F. N. Chukhovskii, D. V. Novikov, T. Hiort, and G. Materlik, Opt. Commun. **209**, 273 (2002).
[8] S. Marchesini and C. S. Fadley, Phys. Rev. B **67**, 024115 (2003).
[9] T. Matsushita, A. Agui, and A. Yoshigoe, Europhys. Lett. **65**, 207 (2004).
[10] Y. Takahashi, E. Matsubara, Y. Kawazoe, K. Takanashi, and T. Shima, Appl. Phys. Lett. **87**, 234104 (2005).
[11] A. Uesaka, K. Hayashi, T. Matsushita, and S. Arai, Phys. Rev. Lett. **107**, 045502 (2011).
[12] F. N. Chukhovskii and A. M. Poliakov, Acta Crystallogr., Sect. A: Found. Crystallogr. **59**, 109 (2003).
[13] F. N. Chukhovskii and A. M. Poliakov, Acta Crystallogr., Sect. A: Found. Crystallogr. **60**, 82 (2004).
[14] B. E. Warren, *X-ray Diffraction* (Dover Publications, Inc, Mineola, NY, 1990).
[15] M. Tegze and G. Faigel, J. Phys.: Condens. Matter **13**, 10613 (2001).
[16] B. Adams, D. V. Novikov, T. Hiort, G. Materlik, and E. Kossel, Phys. Rev. B **57**, 7526 (1998).
[17] B. H. Heise, J. Appl. Phys. **33**, 938 (1962).
[18] M. Tegze, Phys. Rev. B **73**, 214104 (2006).
[19] P. Korecki, D. V. Novikov, M. Tolkiehn, and G. Materlik, Phys. Rev. B **69**, 184103 (2004).
[20] A. Munoz, J. A. Alonso, M. J. Martinez-Lope, M. T. Casais, J. L. Martinez, and M. T. Fernandez-Diaz, Chem. Mater. **13**, 1497 (2001).
[21] K. F. Wang, J. M. Liu, and Z. F. Ren, Adv. Phys. **58**, 321 (2009).
[22] J. Bai, Phys. Rev. B **68**, 144109 (2003).
[23] J. C. Adams and P. N. Swarztrauber, Mon. Weather Rev. **127**, 1872 (1998).